

Correcting pervasive errors in RNA crystallography with Rosetta

Fang-Chieh Chou¹, Parin Sripakdeevong², Rhiju Das^{2,3,4}

¹Department of Chemistry, Stanford University, Stanford, CA 94305, USA

²Biophysics Program, Stanford University, Stanford, CA 94305, USA

³Department of Biochemistry, Stanford University, Stanford, CA 94305, USA

⁴Department of Physics, Stanford University, Stanford, CA 94305, USA

Correspondence should be addressed to R.D. Phone: (650) 723-5976. Fax: (650) 723-6783. E-mail: rhiju@stanford.edu.

Abstract

RNA crystallographic models, our richest sources of RNA structural information, contain pervasive errors due to ambiguities in manually fitting RNA backbones into experimental density maps. To resolve these ambiguities, we have developed a new Rosetta structure prediction tool (ERRASER: Enumerative Rreal-space Refinement Assisted by Electron density under Rosetta) and coupled it to MolProbity validation and PHENIX diffraction-based refinement. On 15 crystallographic datasets for ribozymes, riboswitches, and other RNA domains, ERRASER/PHENIX corrects the majority of identifiable sugar pucker errors, steric clashes, suspicious backbone rotamers, and incorrect bond lengths/angles, while, on average, improving R_{free} correlation to set-aside diffraction data by 0.010. As further confirmation of improved accuracy, the refinement enhances agreement between crystals solved by independent groups and between domains related by non-crystallographic symmetry (NCS). Finally, we demonstrate successful application of ERRASER on coordinates for an entire 30S ribosomal subunit. By rapidly and systematically disambiguating RNA model fitting, ERRASER enables RNA crystallography with significantly fewer errors.

Introduction

Structured RNAs play critical roles in biological processes ranging from genetic regulation to protein synthesis¹⁻². Over the last decade, a renaissance in RNA X-ray crystallography has enabled three-dimensional all-atom modeling of numerous riboswitches, ribozymes, and ribonucleoprotein machines (see, e.g., refs³⁻⁶). Nevertheless, these crystallographic models appear to be rife with small-scale local errors. Most RNA crystallographic data sets have diffraction resolutions between 2.5 and 3.5 Å. At this resolution, phosphates and nucleobases are typically visible in the density map, but the positions of other atoms are often ambiguous⁷⁻⁸, rendering visual fitting into density a challenging task. Detailed analyses of existing crystallographic models have revealed pervasive steric clashes, outlier bond lengths and angles, anomalous sugar geometries, and irregular backbone rotamers⁹⁻¹⁰. At an extreme, ribosome crystallographic models exhibit many hundreds of such errors, as revealed by the MolProbity package¹¹. There is a critical need for tools that can automatically correct these errors in existing RNA crystallographic models and minimize these errors in future crystallographic efforts.

At present, a limited number of computational tools are available for such error correction during structure determination. RNABC⁸ and RCrane⁷ can identify and fix backbone conformer errors in some models. However, these methods anchor phosphates and bases to starting positions determined manually and only correct a subset of errors. Furthermore, neither method uses electron density in the rebuilding process. Automatically rebuilt structures may thus give worse fits to diffraction data (as parameterized in R and R_{free}) than manual starting models and therefore are unlikely to be accepted. Based on the recent advances in Rosetta high-resolution RNA modeling¹²⁻¹³, we have developed a method for Enumerative Real-space Refinement Assisted by Electron density under Rosetta (ERRASER), and combined it with the PHENIX tools for diffraction-guided refinement, with application to 15 structured RNA crystallographic data sets. We report that this automated pipeline resolves the majority of stereochemical and conformer errors in RNA crystallographic models while

retaining or improving correlation to X-ray diffraction data. ERRASER is thus expected to be a powerful tool for increasing the accuracy and information content of our most valuable technology for RNA structural inference.

Results

De novo modeling and the crystallographic refinement problem

Potential problems in manually fitted RNA crystallographic conformations include atom-atom clashes, outlier bond lengths and angles, anomalous sugar geometries, non-planar base-pairing patterns, and backbone conformers that lie outside a curated set of well-characterized 'rotamers'. While not all of these features are necessarily incorrect, their high frequencies in crystallographic models fitted into medium-resolution (2.5-3.5 Å resolution) diffraction maps compared to high-resolution (<2.0 Å) maps suggest that most are due to inaccurate fits^{7-8,10-11}. Thus, for a given experimental electron density map, if an alternative anomaly-free RNA conformation can be found that fits the density as well as (or better than) an anomaly-containing starting model, the refined model is a preferable solution for the crystallographic coordinates¹¹.

We sought to create such models in Rosetta after our observation that RNA *de novo* models produced by Rosetta fragment assembly and full-atom refinement¹²⁻¹³ give negligible errors as assessed by the MolProbity validation package. To help ensure agreement with experimental electron density, we supplemented the Rosetta energy function with an electron density score, recently pioneered for application to electron cryomicroscopy and molecular replacement¹⁴⁻¹⁵. The resulting ERRASER refinement protocol is further combined with diffraction-based refinement by the PHENIX package¹⁶ into a pipeline.

This ERRASER/PHENIX refinement pipeline consists of three stages (Supplementary Fig. 1). First, the starting crystallographic model is refined in PHENIX, with hydrogen atoms added. This step reduces outlier bond angles

substantially, but does not reduce atom-atom clashes on average, as assessed in MolProbity (Table 2). Second, we refine all RNA chains in the asymmetric unit in Rosetta using the ERRASER protocol. The Rosetta all-atom energy function models hydrogen bonding, Lennard-Jones packing, solvation, and torsional preferences, and has been successful in the modeling and design of RNA at near-atomic accuracy¹². A simple continuous minimization of the whole model gives substantial reduction in atom-atom clashes and improvement of base pairing, but does not allow concerted changes of sugar pucker or backbone rotamers. We therefore also include in this stage rebuilding of individual nucleotides. All of a nucleotide's atoms (including its base and sugar) and the atoms up to the previous and next sugar are sampled by exhaustive enumeration and analytical loop closure at sub-Angstrom resolution (see Methods and ref¹⁷⁻¹⁸). To reduce the computational cost to under one CPU-day per data set, only problematic suites flagged by MolProbity are rebuilt in the single nucleotide rebuilding step. In the final stage of the pipeline, the model is refined again in PHENIX, in which the ERRASER models are directly fitted to the experimental data. The details of the protocol are described in the "Methods" section.

A challenging benchmark of RNA crystallographic models

To measure the effectiveness of the ERRASER/PHENIX pipeline, we selected a test set of 15 crystal structures deposited in the PDB (Table 1). The set covers a wide range of RNA lengths (from 27 to 174 nucleotides), diffraction resolutions (from 1.34 to 3.55 Å), R factors (from 0.128 to 0.283), and R_{free} factors (from 0.131 to 0.302), making it representative of the majority of existing problems in RNA crystal structures. For comparison, we also show the results of PHENIX refinement alone. Further, we tested the effectiveness of RNABC and RCrane as alternatives to the ERRASER refinement step in our protocol; these prior approaches have not been comprehensively benchmarked with regards to, e.g., R/R_{free} factors. As a final test, we applied our method to a 30S ribosomal subunit model. These ribosomal results are tabulated and described separately; otherwise, they would dominate the benchmark.

Throughout our study, we took precautions to allow rigorous tests of accuracy improvement through R_{free} calculations and through assessment of consistency between similar segments. First, data set aside for R_{free} calculations were not used in PHENIX refinement or in the electron density map used for Rosetta calculations. Further, non-crystallographic symmetry (NCS) was not assumed for crystals with multiple copies in the asymmetric unit.

To validate the models generated by the ERRASER/PHENIX pipeline, we performed three tests on the starting PDB models and all other models generated by different refinement methods. First, the MolProbity validation tool was used to evaluate the reduction of geometric errors. Second, R/R_{free} factors were calculated to measure the correlation between the models and the experimental diffraction data. Third, we compared the structures of pairs of models with the same or similar RNA sequences in our dataset for their similarity, because they should have similar structures if the models are determined correctly. The results of these tests are described in separate sections below.

ERRASER/PHENIX improves the RNA rotamericity and stereochemistry

Application of the MolProbity suite of validation tools to the fifteen benchmark data sets herein revealed a large number of problems. Each case gave large frequencies of ‘non-rotameric’ backbone conformations (>20), potentially incorrect sugar puckers (>5), unacceptable scores for atom-atom steric clashes (>20), and/or large numbers of outlier bond lengths or bond angles (>10%). We discuss the resolution of these four classes of problems by automated refinement one-by-one.

First, a recent community-consensus analysis, formalized in the MolProbity Suitename algorithm, indicates that 92.4% of RNA backbone ‘suites’ (sets of two consecutive sugar puckers with 5 connecting backbone torsions) fall

into 46 standard rotameric classes¹⁰. Suite conformations in a crystallographic model that lie outside these classes are strong candidates for remodeling. Indeed, the RCrane approach, which specifically samples the 46 rotamers, reduces the number of conformer outliers in 12 of 15 test cases, from an average of 26 outliers per RNA to 14 (Supplementary Table 2 and Fig. 2a). The ERRASER/PHENIX pipeline gives an even larger improvement, reducing the number of outliers in all 15 test cases and giving a smaller average number of outliers, 11 per RNA (Table 2 and Fig. 2a). The result, a two-fold reduction of outliers over the deposited conformations, is particularly striking since no information on the SuiteName 46-rotamer library is used in the Rosetta energy function or during sampling.

The success of ERRASER to give accurate rotameric conformers appears to be largely due to extra information provided by the Rosetta all-atom energy function. In a few cases, the diffraction data are at reasonably high resolution (e.g., for a guanine riboswitch 1U8D and a thiamine pyrophosphate riboswitch 2GDI, with diffraction resolutions of 1.95 Å and 2.05 Å, respectively; Fig. 1a and 1b), and the ERRASER-fitted conformer shows visually better agreement with the electron density (Fig. 1a and 1b). However, in most cases, the starting and remodeled conformer fit the density equally well by visual inspection; here, the ambiguity in the density map has been resolved by the Rosetta energy function. For example, Fig. 1c shows an 8-nucleotide hairpin segment from coordinates 2OIU (L1 Ribozyme Ligase; 2.6 Å diffraction resolution) exhibiting only 2 rotameric conformations in 7 suites. This segment is slightly improved (3 rotameric suites) when using RCrane/PHENIX. The ERRASER/PHENIX approach, which allows for refinement of base and phosphate positions and discrimination by the Rosetta energy function, gives a different solution that fits the electron density. 5 out of 7 suites in the ERRASER solution are assigned to be standard rotamers by SuiteName (blue letters in Fig. 1c). Interestingly, four of the new suites are 1a, the most common rotamer, although this was not recognized in the original fit or by RCrane.

Beyond rotamericities of backbone suite conformations, MolProbity uses the distance between the glycosidic bond vector (C1'–N1/9) and the following (3') phosphate to locate potential sugar pucker errors. The number of such potentially incorrect puckers increases with worse diffraction resolution (Fig. 2b), reflecting the difficulty of assigning sugar conformations into low-resolution density maps. ERRASER/PHENIX automatically reduces the number of potentially incorrect puckers, making the number almost resolution independent. Indeed while only one test case (2A43, the highest resolution data set, 1.34 Å) had zero MolProbity-flagged pucker errors in starting PDB coordinates, 10 of the 15 cases give no pucker errors after ERRASER/PHENIX refinement.

In addition, ERRASER/PHENIX reduces the steric clashes in the RNA, guided by the Lennard-Jones repulsion terms in the Rosetta energy function. Fig. 1d shows an example in a cyclic-di-GMP riboswitch model 3IWN; the majority of clashes are removed. Remaining clashes are mostly between the RNA and a ligand, which is not currently remodeled by ERRASER. Over the entire benchmark, the MolProbity clashscore, which provides an assessment of atom-atom steric overlaps, is reduced from an average of 17.3 to 10.9. Other refinement approaches (RCrane/PHENIX and RNABC/PHENIX) that use less stringent or no steric criteria give higher average clashscores (Supplementary Table 1).

The final feature assessed by MolProbity is the frequency of outlier bond distances and angles in the crystallographic models, which have starting frequencies of 1.0% and 19.2% in starting PDB coordinates. These values are brought to 0% and 0.32% by the ERRASER/PHENIX refinement. Other methods give equal or worse values (Table 2, Supplementary Table 3).

ERRASER/PHENIX improves RNA base-pairing geometry

ERRASER/PHENIX visually improves the base pairing patterns of the RNA models, enhancing the co-planarity of interacting bases. For example, Fig. 1e shows a helical region in 3P49, a structure solved at 3.55 Å resolution. At

this resolution, accurate positioning of base planes into the electron density map is difficult. Manual fits give base pairs that are buckled or twisted compared to geometries seen in higher-resolution crystallographic models¹⁹. RNABC and RCrane hold the base positions fixed during rebuilding and are thus unable to improve the base pair planarity. On the other hand, ERRASER/PHENIX improves the planarity of the base-pairs, likely due to the hydrogen bonding potential included in the Rosetta energy function. Independent base-pair validation tools – which, like MolProbity, would permit unbiased assessment of improvement – are not currently available. However, we applied the base-pair assignment method MC-Annotate²⁰ and noted that the refined structures gave a higher number of automatically assigned base-pairs than the starting PDB models in 10 out of 15 cases (Supplementary Table 4). For the 3P49 case, ERRASER/PHENIX increases the number of base-pairs from 44 in the PDB model to 60. Other methods (RCrane/PHENIX and RNABC/PHENIX) lead to smaller improvements in this case, each giving 49 base-pairs.

ERRASER/PHENIX leads to similar or lower R_{free} and R factors

Any method for improvement of geometric features will not be of practical use if the resulting models give worse fits to the diffraction data, as parameterized by R factor (R) and free R factor (R_{free}) values. In particular, avoiding increases in R_{free} is critical for demonstrating that overfitting of the experimental data has not occurred²¹. Table 1 summarizes R and R_{free} of the starting PDB models and the final model after automated refinement. Diffraction-guided refinement by PHENIX alone consistently drops both R and R_{free} , improving R_{free} in 12 out of 15 cases; the average changes are $\Delta R = -0.023$ and $\Delta R_{free} = -0.008$, respectively (Table 1; see also Fig. 2c). RCrane/PHENIX and RNABC/PHENIX give slightly worse results, e.g., the average ΔR_{free} is -0.005 for RCrane and -0.007 for RNABC (see Supplementary Table 6), underscoring the difficulty of maintaining fits to diffraction data upon rebuilding.

The ERRASER/PHENIX pipeline gives an average $\Delta R = -0.019$ and an improved average $\Delta R_{\text{free}} = -0.010$; in 10 of 15 cases ERRASER/PHENIX gives better R_{free} than the PDB models (Supplementary Table 5, 6 and Fig. 2c). Checking the test cases individually, we find 3 cases where ERRASER/PHENIX leads to significant R_{free} improvement (better than -0.005) compared to PHENIX alone, and 12 cases in which the two methods give similar R_{free} (within ± 0.005). We conclude that ERRASER prevents worse model fits to independent diffraction data and, in some cases, offers a measurable improvement.

Independent tests of ERRASER/PHENIX accuracy

In addition to the geometric and experimental consistency checks above, we sought independent tests of accuracy for the ERRASER/PHENIX-refined models. While crystallographic models are usually considered “gold standards” for structure prediction problems, we are faced here with imperfect crystallographic models which cannot act as references. We reasoned that pairs of models with the same or similar RNA sequences should give similar conformations at corresponding nucleotides, and an accurate refinement procedure should maintain or improve this similarity.

We drew nine such structural pairs from three categories: two copies present in the asymmetric unit (5 cases; note that NCS was not assumed in refinement); models of the same sequences determined by independent groups at different resolutions (3 cases); and the conserved regions of two aptamer domains in glycine riboswitch (1 case, 3P49). Table 3 summarizes the results of the similarity comparison of the torsion angles of each nucleotide pair, sugar pucker assignment and the RMSD in torsional space for these structure pairs. On average, PHENIX alone improves the similarity metrics in 6 of 9 cases compared to the PDB models. In all 9 cases, ERRASER/PHENIX improves these metrics compared to the PDB models. Some of these improvements in the similarity of local geometries are striking, as shown in Fig. 1f. Combined with the R_{free} test above, the improved

consistency between same or homologous RNAs gives additional confidence that automated ERRASER/PHENIX refinement improves the accuracy of crystallographic models.

Final test: application to a 30S ribosomal subunit

As a final test of our ERRASER/PHENIX pipeline, we applied it to a recently published crystallographic model of the 30S ribosomal subunit of *Thermus thermophilus*, 3OTO²². This structural model has 1,522 nucleotides in its RNA component, with a resolution of 3.69 Å, and it takes 3 CPU-days to refine this model in ERRASER/PHENIX. The validation results of the ERRASER/PHENIX model as well as the PDB, PHENIX, RCrane/PHENIX and RNABC/PHENIX models are shown in Table 4. PHENIX alone gives modest improvements in all error categories; only R_{free} increases slightly from 0.231 to 0.236. The ERRASER/PHENIX pipeline partially rescues R_{free} to 0.235. Most importantly, ERRASER/PHENIX significantly reduces all classes of geometric errors as assessed by MolProbity, lowering the clashscore from 41.6 to 12.3, the number of potentially incorrect puckers from 35 to 4, and the number of outlier conformers from 281 to 141. Furthermore, the bond length and bond angle outliers are both reduced from 0.07% to 0%. Finally, the number of base-pairs assigned by MC-Annotate increases from 561 to 656 after the ERRASER/PHENIX pipeline. Other methods lead to similar R/R_{free} , and similar or worse reduction of errors in all categories compared to ERRASER/PHENIX.

Discussion

Due to the difficulty of manually fitting RNA structures into crystallographic electron density maps, there is a critical need for automatic and objective structure refinement tools that reduce model anomalies while maintaining good fits to diffraction data. The recent development of atomic-resolution RNA modeling in Rosetta¹²⁻¹³ offers a potential solution to this challenge, and recent studies on solving the crystallographic phase problem by molecular replacement supplemented by Rosetta^{14,23-24} provide precedents for coupling structure

prediction to crystallography. In this study, we have demonstrated that a new Rosetta-based protocol called ERRASER, when combined with the powerful MolProbity and PHENIX tools, indeed leads to consistent and substantial improvement of backbone rotamericities, sugar geometry, steric quality, and bond geometries. The majority of identifiable geometric errors are resolved in all cases. Importantly, the refined models give similar or better fits to the diffraction data in all cases. Additional tests involving automated annotation of base-pairs and systematic cross-comparison of independently refined structure pairs, give further confidence that this automated pipeline consistently increases the accuracy of RNA crystallographic models. Finally, the successful application of this method on the 30S ribosomal subunit has proven that it can be generally applied to all types of RNA crystallographic refinement problems.

The ERRASER/PHENIX pipeline should be immediately useful for RNA crystallographers. A single CPU-day of automated ERRASER refinement to correct geometric ambiguities and errors is reasonably small compared to the weeks of manual efforts required to phase and build coordinates for RNA diffraction data. In addition, several extensions of ERRASER are under investigation. Enumerative rebuilding of RNA/protein and RNA/ligand interfaces, Patterson-based scoring during Rosetta RNA modeling, more aggressive rebuilding to reduce dependence on starting models, and acceleration through parallelization appear to be feasible. As ERRASER and other high-resolution modeling tools become widely used by structural biologists, we look forward to a new generation of higher accuracy RNA crystallography.

Acknowledgements

We thank J. S. Richardson for suggesting this problem, C. L. Zirbel and N. B. Leontis for suggestions on base-pairing validation, the Das lab for comments on the manuscript and members of the Rosetta community for discussions and code sharing. Calculations were performed on the BioX² cluster (NSF award CNS-0619926).

This work is supported by a Burroughs-Wellcome Career Award at Scientific Interface (R.D.), a Study Abroad Scholarship of Taiwan Government (F.C.C.), and the C. V. Starr Asia/Pacific Stanford Graduate Fellowship (P.S.).

Author Contributions

F.C.C., P.S. and R.D. designed the research. F.C.C. implemented the methods and analyzed the results. P.S. provided the stepwise assembly code and assisted in data analysis. F.C.C. and R.D. prepared the manuscript.

Competing Financial Interests

The authors declare no competing financial interests.

Methods

Overview of the ERRASER/PHENIX pipeline

The ERRASER/PHENIX pipeline involves three major stages (Supplementary Fig. 1). The starting model deposited in the PDB was first refined in PHENIX (v1.7.1-743). The refined model and electron-density map (setting aside the data for free R factor calculations; see Supplementary Methods) were then passed into Rosetta for a three-step real-space refinement. First, all torsion angles and all backbone bond lengths and bond angles were subjected to continuous minimization under the Rosetta high-resolution energy function. An electron density correlation score ensured that the minimized structures retain good fits to the density map. Suites with non-rotameric backbone conformations were then identified in MolProbity's Suitename application (v0.3.070628)¹⁰. These suites were rebuilt by single-nucleotide StepWise Assembly (SWA) in a one-by-one fashion. If SWA found a lower-energy alternative structure of the rebuilt nucleotide, this new conformation was accepted. After the nucleotides were rebuilt, the new model was then minimized again in Rosetta to obtain the final ERRASER model.

This model was again refined in PHENIX against diffraction data to obtain the final ERRASER/PHENIX model. The code is being made available in the next Rosetta release (3.4), which will be freely available to academic users at <http://www.rosettacommons.org>. Prior to release, this code will be gladly provided to academic users upon request. Details, example command lines, and accelerations used for the refinement of 30S ribosomal subunit are given in Supplementary Methods.

R and R_{free} calculation

For consistency, R and R_{free} values of all the models were calculated using `phenix.model_vs_data`²⁵. For the starting models, most of the PHENIX-calculated R and R_{free} were similar to the values shown in the PDB header; both are reported in Supplementary Table 5 and 6. In the main text, we have reported PHENIX-calculated R and R_{free} to permit comparisons across the refinement benchmark.

Similarity analysis test

The similarities of the local geometries between similar structural models (Table 3, Supplementary Table 7 and 8) were evaluated as follows. If differences between the torsion angles (α , β , γ , δ , ϵ , ζ , χ) of each nucleotide pair were all smaller than 40°, we counted the pair as a similar nucleotide pair. If the difference of the δ angles of a nucleotide pair was smaller than 20°, then we assigned the pair as having similar sugar pucker. Finally, RMSDs of all the torsion angles (in degrees) between the model pairs were calculated as an indicator of the model similarity in the torsional space.

Other tools

RCrane⁷ (v1.01) and RNABC⁸ (v1.11) were combined with PHENIX in the same way as the ERRASER/PHENIX pipeline, by substituting the ERRASER stage with RCrane and RNABC, respectively. Since RNABC rebuilt only one nucleotide per run, a python script was used to achieve automatic rebuilding of all nucleotides. In MolProbity¹¹

(internal reference 3.18), the multichart command line tool was used to generate multi-criterion charts that gave all the five metrics for structural model evaluations discussed in the main text. MC-Annotate²⁰ (v1.6.2) was used to assign base-pairs in starting and refined models. All molecular images in this work were prepared using PyMol, except Fig. 1c, which used MolProbity¹¹ and KiNG²⁶.

References

1. Ban, N., Nissen, P., Hansen, J., Moore, P.B. & Steitz, T.A. The complete atomic structure of the large ribosomal subunit at 2.4 Å resolution. *Science* **289**, 905-920 (2000).
2. Gesteland, R.F., Cech, T. & Atkins, J.F. (eds.). *The RNA world: the nature of modern RNA suggests a prebiotic RNA world*, (Cold Spring Harbor Laboratory Press, Cold Spring Harbor, N.Y., 2006).
3. Butler, Ethan B., Xiong, Y., Wang, J. & Strobel, Scott A. Structural Basis of Cooperative Ligand Binding by the Glycine Riboswitch. *Chemistry & Biology* **18**, 293-298 (2011).
4. Dunkle, J.A. et al. Structures of the Bacterial Ribosome in Classical and Hybrid States of tRNA Binding. *Science* **332**, 981-984 (2011).
5. Leung, A.K.W., Nagai, K. & Li, J. Structure of the spliceosomal U4 snRNP core domain and its implication for snRNP biogenesis. *Nature* **473**, 536-539 (2011).
6. Stahley, M.R. & Strobel, S.A. Structural Evidence for a Two-Metal-Ion Mechanism of Group I Intron Splicing. *Science* **309**, 1587-1590 (2005).
7. Keating, K.S. & Pyle, A.M. Semiautomated model building for RNA crystallography using a directed rotameric approach. *Proc. Natl. Acad. Sci. USA* **107**, 8177-8182 (2010).
8. Wang, X. et al. RNABC: forward kinematics to reduce all-atom steric clashes in RNA backbone. *J. Math. Biol.* **56**, 253-278 (2008).
9. Murray, L.J.W., Arendall, W.B., Richardson, D.C. & Richardson, J.S. RNA backbone is rotameric. *Proc. Natl. Acad. Sci. USA* **100**, 13904-13909 (2003).
10. Richardson, J.S. et al. RNA backbone: Consensus all-angle conformers and modular string nomenclature (an RNA Ontology Consortium contribution). *RNA* **14**, 465-481 (2008).
11. Chen, V.B. et al. MolProbity: all-atom structure validation for macromolecular crystallography. *Acta Cryst. D* **66**, 12-21 (2010).
12. Das, R., Karanicolas, J. & Baker, D. Atomic accuracy in predicting and designing noncanonical RNA structure. *Nat. Methods* **7**, 291-294 (2010).
13. Das, R. & Baker, D. Automated de novo prediction of native-like RNA tertiary structures. *Proc. Natl. Acad. Sci. USA* **104**, 14664-14669 (2007).
14. DiMaio, F. et al. Improved molecular replacement by density- and energy-guided protein structure optimization. *Nature* **473**, 540-543 (2011).
15. DiMaio, F., Tyka, M.D., Baker, M.L., Chiu, W. & Baker, D. Refinement of Protein Structures into Low-Resolution Density Maps Using Rosetta. *J. Mol. Biol.* **392**, 181-190 (2009).
16. Adams, P.D. et al. PHENIX: a comprehensive Python-based system for macromolecular structure solution. *Acta Cryst. D* **66**, 213-221 (2010).
17. Sripakdeevong, P., Kladwang, W. & Das, R. An enumerative stepwise ansatz enables atomic-accuracy RNA loop modeling. *Proc. Natl. Acad. Sci. USA*, in press.

18. Mandell, D.J., Coutsias, E.A. & Kortemme, T. Sub-angstrom accuracy in protein loop reconstruction by robotics-inspired conformational sampling. *Nat. Methods* **6**, 551-552 (2009).
19. Stombaugh, J., Zirbel, C.L., Westhof, E. & Leontis, N.B. Frequency and isostericity of RNA base pairs. *Nucleic Acids Res.* **37**, 2294-2312 (2009).
20. Gendron, P., Lemieux, S. & Major, F. Quantitative analysis of nucleic acid three-dimensional structures. *J. Mol. Biol.* **308**, 919-936 (2001).
21. Brunger, A.T. Free R value: A novel statistical quantity for assessing the accuracy of crystal structures. *Nature* **355**, 472-475 (1992).
22. Demirci, H. et al. Modification of 16S ribosomal RNA by the KsgA methyltransferase restructures the 30S subunit to optimize ribosome function. *RNA* **16**, 2319-2324 (2010).
23. Das, R. & Baker, D. Prospects for de novo phasing with de novo protein models. *Acta Cryst. D* **65**, 169-175 (2009).
24. Qian, B. et al. High-resolution structure prediction and the crystallographic phase problem. *Nature* **450**, 259-264 (2007).
25. Afonine, P.V. et al. phenix.model_vs_data: a high-level tool for the calculation of crystallographic model and data statistics. *J. Appl. Crystallogr.* **43**, 669-676 (2010).
26. Chen, V.B., Davis, I.W. & Richardson, D.C. KING (Kinemage, Next Generation): A versatile interactive molecular and scientific visualization program. *Protein Sci.* **18**, 2403-2409 (2009).

Table 1. Benchmark test set of 15 structural models and corresponding R/R_{free}

Name	PDB ID	RNA length ^a	Resolution (Å)	R			R _{free}		
				PDB	PHENIX	ERRASER / PHENIX	PDB	PHENIX	ERRASER / PHENIX
RNA Pseudoknot	2A43	26	1.34	0.135	0.119	0.123	0.183	0.157	0.158
Lysine Riboswitch	3DIL	174	1.9	0.188	0.173	0.173	0.220	0.207	0.206
TPP Riboswitch	2GDI	80*2	2.05	0.207	0.194	0.196	0.238	0.232	0.235
Hammerhead Ribozyme	2QUS	69*2	2.4	0.192	0.199	0.202	0.265	0.271	0.266
L1 Ribozyme Ligase	2OIU	71*2	2.6	0.204	0.195	0.207	0.234	0.237	0.236
TPP Riboswitch	2CKY	77*2	2.9	0.195	0.165	0.178	0.250	0.243	0.234
SAM-I Riboswitch	2GIS	94	2.9	0.264	0.217	0.219	0.269	0.260	0.262
SAM-III Riboswitch	3E5E	53	2.9	0.224	0.195	0.196	0.254	0.250	0.253
FMN Riboswitch	3F2Q	112	2.95	0.207	0.207	0.209	0.265	0.264	0.266
Prohead RNA	3R4F	66	3.5	0.252	0.219	0.219	0.290	0.278	0.277
Glycine Riboswitch	3P49	169	3.55	0.283	0.219	0.218	0.302	0.278	0.271
Guanine Riboswitch	1U8D	68	1.95	0.188	0.178	0.178	0.225	0.211	0.211
Guanine Riboswitch	1Y27	68	2.4	0.235	0.217	0.220	0.265	0.280	0.270
c-di-GMP Riboswitch	3MXH	92	2.3	0.239	0.198	0.195	0.287	0.257	0.252
c-di-GMP Riboswitch	3IWN	93*2	3.2	0.223	0.197	0.221	0.294	0.291	0.292
Average Drop ^b					-0.023	-0.019		-0.008	-0.010
Equal or better than PDB					14 / 15	12 / 15		12 / 15	11 / 15
Within 0.005 of PDB or better					14 / 15	14 / 15		13 / 15	15 / 15

^a The length of RNA component of the molecule. “*2” indicates 2 copies in the asymmetric unit.

^b compared to PDB values.

Table 2. MolProbity analysis of the benchmark set

PDB ID	Clashscore			Potentially incorrect puckers			Outlier conformers			Outlier angles (%)		
	PDB	PHENIX	ERRASER /PHENIX	PDB	PHENIX	ERRASER /PHENIX	PDB	PHENIX	ERRASER /PHENIX	PDB	PHENIX	ERRASER /PHENIX
2A43	1.19	1.19	1.19	0	0	0	1	1	1	34.62	0	0
3DIL	1.40	5.6	5.95	4	2	0	18	13	13	6.32	2.3	1.72
2GDI	4.98	8.81	5.17	8	3	2	23	18	12	6.96	0.63	0.63
2QUS	12.97	15.21	8.72	9	6	0	35	29	15	35.29	1.47	0
2OIU	8.48	17.82	6.09	6	3	0	29	24	7	45.77	2.82	0
2CKY	20.01	27.14	8.12	18	9	2	64	53	17	57.79	1.95	0
2GIS	42.85	30.7	21.75	8	7	0	21	19	9	9.57	1.06	0
3E5E	5.09	10.74	7.91	2	1	0	6	6	3	21.15	0	0
3F2Q	9.47	5.85	3.34	3	2	0	22	16	7	6.48	0.93	0.93
3R4F	49.62	93.1	27.84	5	5	0	16	25	9	7.58	1.52	0
3P49	17.56	20.84	20.13	19	11	4	73	56	28	18.34	1.18	0
1U8D	14.02	9.25	11.35	3	2	0	4	4	0	14.93	4.48	1.49
1Y27	6.82	13.63	6.36	4	2	0	13	13	7	11.94	2.99	0
3MXH	8.45	6.89	7.56	1	1	1	8	7	8	2.2	0	0
3IWN	56.02	57.79	22.3	23	17	2	52	67	26	9.14	12.9	0
Average	17.26	21.64	10.92	7.53	4.73	0.73	25.67	23.40	11.07	19.21	2.28	0.32
Equal or better than PDB		5 / 15	11 / 15		15 / 15	15 / 15		13 / 15	15 / 15		14 / 15	15 / 15

Table 3. Similarity comparison for RNA models of the same or similar sequences

Chain 1	Chain 2	Similar nucleotides (%) ^a			Similar puckers (%) ^b			Torsional RMSD (degrees) ^c		
		PDB	PHENIX	ERRASER /PHENIX	PDB	PHENIX	ERRASER /PHENIX	PDB	PHENIX	ERRASER /PHENIX
2GDI_1	2GDI_2	79.49	87.18	88.46	97.44	100.00	97.44	25.07	23.45	24.56
2OIU_1	2OIU_2	42.25	45.07	66.20	87.32	94.37	95.77	44.46	42.14	35.24
2QUS_1	2QUS_2	63.24	72.06	82.35	92.65	91.18	94.12	46.24	43.23	29.27
3IWN_1	3IWN_2	50.65	35.06	66.23	94.81	93.51	96.10	42.62	45.22	38.58
3IWN_1	3MXH	53.25	51.95	64.94	85.71	89.61	93.51	48.08	46.04	40.22
3IWN_2	3MXH	46.75	45.45	57.14	81.82	90.91	89.61	51.97	50.86	42.79
3P49_1	3P49_2	34.21	34.21	68.42	84.21	94.74	94.74	50.40	49.60	36.10
2CKY_1	2CKY_2	59.74	62.34	79.22	90.91	98.70	97.40	32.13	32.89	30.73
1U8D	1Y27	68.85	68.85	85.25	95.08	93.44	98.36	36.14	35.55	23.69
Average		55.38	55.80	73.13	89.99	94.05	95.23	41.90	41.00	33.46
Equal or better than PDB			6 / 9	9 / 9		6 / 9	9 / 9		7 / 9	9 / 9

^a Nucleotide pair in which the differences between all torsion angles are smaller than 40°.

^b Nucleotide pair in which the difference between δ angle is smaller than 20°.

^c RMSD of all torsion angles between the model pair.

Table 4. Refinement results for 3OTO, a crystallographic model of a 30S ribosomal subunit

	PDB	PHENIX	RNABC/ PHENIX	RCrane/ PHENIX	ERRASER /PHENIX
RNA length	1,522				
Resolution (Å)	3.69				
R	0.175	0.176	0.176	0.173	0.181
R _{free}	0.231	0.236	0.238	0.236	0.235
Clashscore	41.6	19.29	18.29	19.52	12.73
Potentially incorrect puckers	35	35	35	20	4
Outlier conformers	281	258	261	158	141
Outlier bonds (%)	0.07	0	0	0	0
Outlier angles (%)	0.07	0.07	0.07	0.99	0
# of base-pairs ^a	561	566	561	562	656

^a Base-pairs counted using MC-Annotate.

Figure Captions

Figure 1. Error correction of RNA crystallographic models by ERRASER/PHENIX. **(a, b)** Conformer correction and improved fit to the density by ERRASER/PHENIX on **(a)** nucleotides 62-64, chain A of 1U8D (guanine riboswitch) and **(b)** nucleotides 53-56, chain X of 2GDI (TPP riboswitch). The conformer assignments by Suitename are shown at each suite. “!!” stands for an outlier suite. Electron density map is shown in gray mesh. Red: PDB model. Blue: ERRASER/PHENIX model. **(c)** Conformer correction by ERRASER/PHENIX on nucleotides 27-34, chain Q of 2OIU (L1 ribozyme ligase). Red: PDB model. Green: RCrane/PHENIX model. Blue: ERRASER/PHENIX model. **(d)** Clash reduction by ERRASER/PHENIX in chain A of 3IWN (c-di-GMP riboswitch). Red dots represent unfavorable clashes in the models. Left: PDB model. Right: ERRASER/PHENIX model. **(e)** Base-pairing improvement by ERRASER/PHENIX on nucleotides 1-6 and 66-71, chain A of 3P49 (glycine riboswitch). Left: PDB model. Right: ERRASER/PHENIX model. **(f)** Improved similarity of local geometry by ERRASER/PHENIX between chain A and chain B for nucleotides 55-57 (the three nucleotides on the right) of 2QUS (hammerhead ribozyme). The base-pairing partners of these nucleotides are also shown in the figure. Top: PDB model. Bottom: ERRASER/PHENIX model. Brown: chain A. Cyan: chain B.

Figure 2. Improvements of the crystallographic models by automated refinement tools across the test cases. Compared to the PDB models, ERRASER/PHENIX gives the lowest number of outlier conformers in 14 of 15 cases, the lowest number of potentially incorrect sugar puckers in all cases, and similar or lower R_{free} in all cases.

Figure 1

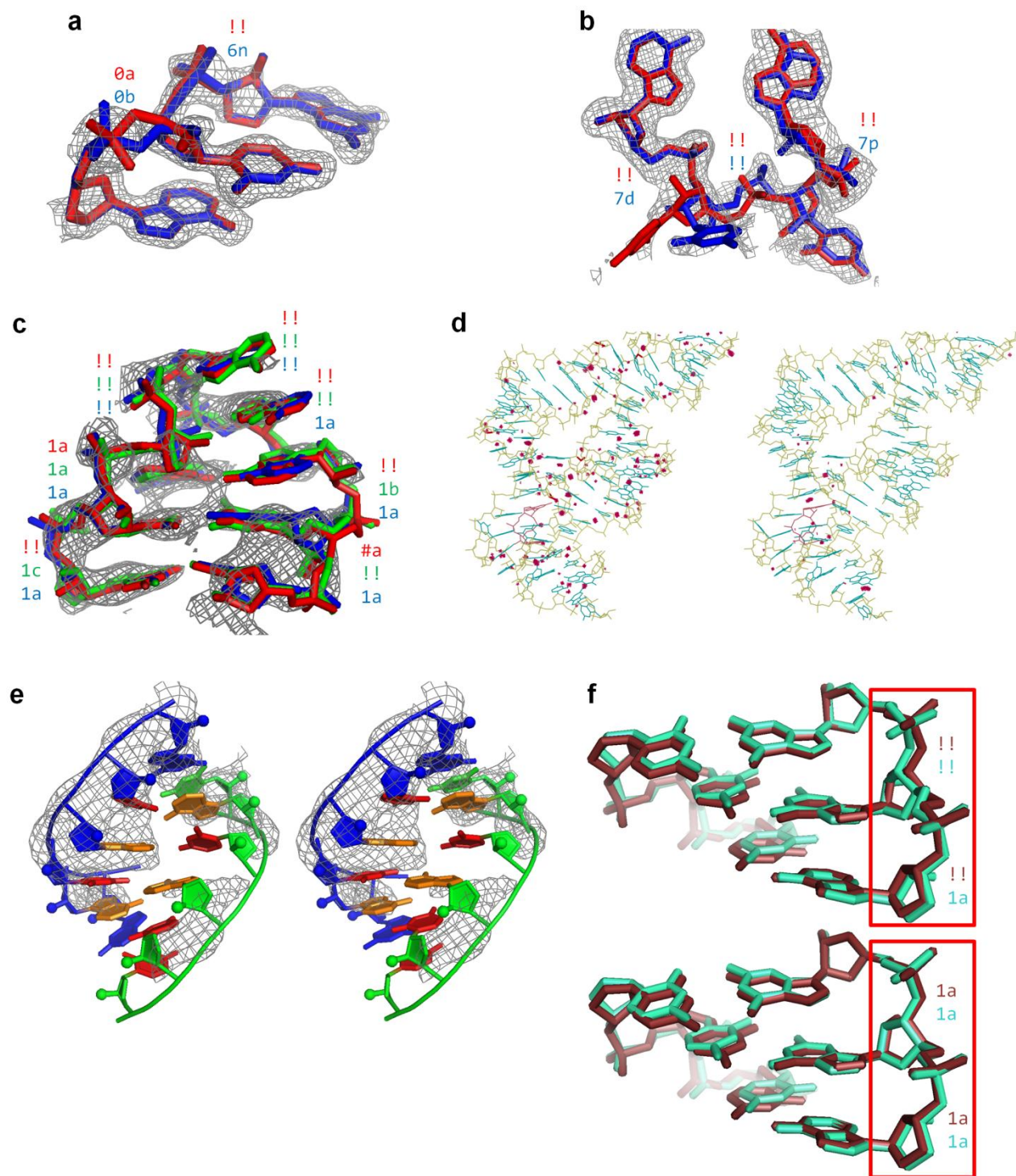
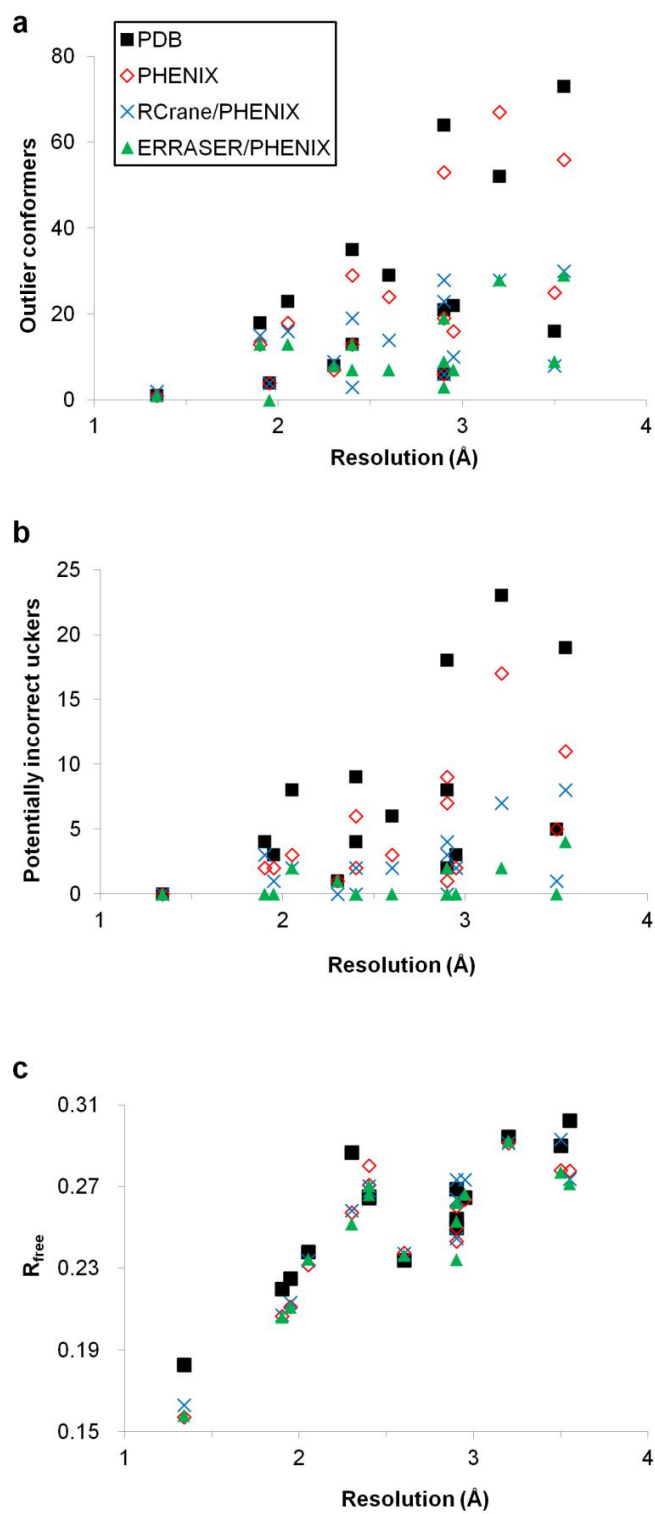


Figure 2



Supplementary Information for “Correcting pervasive errors in RNA crystallography with Rosetta”

Fang-Chieh Chou¹, Parin Sripakdeevong², Rhiju Das^{2,3,4}

¹Department of Chemistry, Stanford University, Stanford, CA 94305, USA

²Biophysics Program, Stanford University, Stanford, CA 94305, USA

³Department of Biochemistry, Stanford University, Stanford, CA 94305, USA

⁴Department of Physics, Stanford University, Stanford, CA 94305, USA

Correspondence should be addressed to R.D. Phone: (650) 723-5976. Fax: (650) 723-6783. E-mail: rhiju@stanford.edu.

This document contains Supplementary Methods, 9 Supplementary Tables and 1 Supplementary Figure.

Supplementary Methods

The new Rosetta module, ERRASER

The ERRASER protocol consisted of three steps: an initial whole structure minimization, followed by single nucleotide rebuilding, and finally a second whole structure minimization. Before passing the models into ERRASER, the PHENIX-generated pdb files were converted to the Rosetta format using a python script `make_rna_rosetta_ready.py`, distributed with Rosetta. All the protein components, ligands and modified nucleotides are removed from the model, because current Rosetta modeling can only handle standard RNA nucleotides. To avoid anomalies in refitting, we held fixed the positions of the nucleotides that were bonded or in van der Waals contact with these removed atoms or with other nucleotides though crystal contact during the next ERRASER step.

Throughout the ERRASER refinement, an electron density score was added to the energy function to ensure that the rebuilt structural models had a good fit to the experimental data. The electron density scoring in our method is slightly different from the one published recently¹⁻². Instead of calculating the density profile of the model every time we rescore the model, we pre-calculated the correlation between the density of a single atom and the experimental density in a fine grid. The score was defined as the negative of the sum of the atomic numbers of all the heavy atoms in the model times this rapidly computed real-space correlation coefficient. We demonstrated this new density scoring term, named `elec_dens_atomwise`, to be an order of magnitude faster than the one in the previous Rosetta release, therefore reducing the total computational time of our method significantly. To accommodate the change of our energy function caused by the electron density energy constraint, we also modified the weights in the original scoring function (see below).

After the whole structure minimization, we used the Suitename program (v0.3.070628) to analyze the obtained models. All nucleotides assigned as outlier conformers or with suiteness smaller than 0.1 were identified as

problematic and were rebuilt in subsequent Rosetta single nucleotide rebuilding. Furthermore, because the single nucleotide rebuilding region in Rosetta did not match the definition of a “suite”, we rebuilt both the selected nucleotide and the nucleotide preceding it to cover the whole suite.

The single nucleotide rebuilding step used in our method was based on a modified SWA algorithm in which the RNA chain was closed using analytical loop closure³. For nucleotides at chain termini, the original SWA sampling was used since no chain closure was required. For rebuilding nucleotides inside the RNA chain, we first created a chain break between O3' and P in the lower suite of the rebuilding nucleotide. Then we sampled all possible torsion angles for $\epsilon_i, \zeta_i, \alpha_i, \delta_i, \alpha_{i+1}$, in 20° steps. For each sampled conformation, analytical loop closure was applied to close the chain and determine the remaining 6 torsions ($\beta_i, \gamma_i, \epsilon_{i+1}, \zeta_{i+1}, \beta_{i+1}, \gamma_{i+1}$). The glycosidic torsion χ_i was sampled after chain closure, and the generated models were further minimized in Rosetta. To reduce the computational expense, we only searched conformations that were within 2.0 Å RMSD with respect to the starting models.

After the conformational search, 30 lowest energy models were kept and further minimized under the constraint of the Rosetta `linear_chainbreak` energy term to ensure that the chain break was closed properly in the final model. To ensure that the rebuilt models retained a good fit to the electron density map, if a minimized model had an electron-density-score less than 90% of the electron-density-score of the input model, the model was discarded. Finally the best scored model was outputted as the new model for the RNA. If no proper new model could be found (e.g. all rebuilt models had electron-density-score less than 90% of the score of input model), then the program kept the starting model of that nucleotide. In the rebuilding process, the candidate nucleotides were rebuilt sequentially from the 5'-end to 3'-end of the RNA sequence.

After all the problematic nucleotides were rebuilt, we minimized the whole model again to further reduce any

bond length/bond angle errors that might have occurred in the rebuilding process, and to improve the overall energy of the model. The coordinates of the RNA atoms in the PHENIX model were then substituted by the new coordinates in our new Rosetta-rebuilt model to give the final ERRASER output.

The three ERRASER steps discussed above were wrapped into a python script `eraser.py` and can be performed automatically. The user needs to input a starting pdb file, a ccp4 map file, the resolution of the map, a list of nucleotides needed to be held fixed during refinement due to their interaction with removed atoms, and cut points existing in the starting pdb file (where the nucleotide next to it is not connected to itself).

A sample ERRASER command line used for the refinement of 3IWN is shown below:

```
eraser.py -pdb 3IWN.pdb -map 3iwn.ccp4 -map_res 3.2 -fixed_res A37 A58 A59 A60  
A61 A62 A63 A64 A65 A66 A67 B137 B158 B159 B160 B161 B162 B163 B164 B165 B166  
B167 -cutpoint_open A93
```

Here 3IWN.pdb is the name of PHENIX refined model, 3iwn.ccp4 is the name of ccp4 density map file, -map_res tag gives the resolution of the density map, and -fixed_res and -cutpoint_open tags specify the nucleotides we want to keep untouched in the and the cutpoint nucleotides, respectively. "A37" means the 37th nucleotide of chain A in the pdb file.

Examples of the automatically generated Rosetta command lines by the python script are shown below:

(1) Full structure minimization

```
rna_pdb_minimizing.<exe> -database <database path> -native <pdb name>  
-force_field_file edensity_min -vary_geometry true -fixed_res 37 58 59 60 61 62  
63 64 65 66 67 130 151 152 153 154 155 156 157 158 159 160 -edensity:mapfile <map  
file> -edensity:mapreso 3.2 -edensity:realign no
```

(2) Single nucleotide rebuilding with analytical chain closure

```
rna_swa_analytical_loop_close.<exe> -algorithm rna_resample_test -s <pdb name>  
-out:file:silent blah.out -no_o2star_screen true -cluster:radius 0.3
```

```

-native_edensity_score_cutoff 0.9 -sampler_native_rmsd_screen true
-sampler_native_screen_rmsd_cutoff 2.0 -num_pose_kept 30
-allow_chain_boundary_jump_partner_right_at_fixed_BP true -sample_res 4
-cutpoint_closed 4 -database <database path> -fasta <fasta file> -input_res 1-3
5-186 -input_res 1-3 5-186 -fixed_res 1-3 5-186 -fixed_BP_list
NOT_ASSERT_IN_FIXED_RES 1-186 -alignment_res 1-186 -rmsd_res 186 -native <native
pdb name> -force_field_file edensity_test -edensity:mapfile <map file>
-edensity:mapreso 3.2 -edensity:realign no -cutpoint_open 93

```

(3) Single nucleotide rebuild at terminal nucleotides

```

rna_swa_test.<exe> -algorithm rna_resample_test -s <pdb name> -out:file:silent
blah.out -no_o2star_screen true -cluster:radius 0.3
-native_edensity_score_cutoff 0.9 -sampler_native_rmsd_screen true
-sampler_native_screen_rmsd_cutoff 2.0 -num_pose_kept 30 -fast false
-skip_minimize false -allow_chain_boundary_jump_partner_right_at_fixed_BP true
-sample_res 93 -database /home/fcchou/minirosetta_database -fasta <fasta file>
-input_res 1-186 -fixed_res 1-92 94-186 -fixed_BP_list NOT_ASSERT_IN_FIXED_RES
1-186 -alignment_res 1-186 -rmsd_res 186 -native <native pdb name>
-force_field_file edensity_test -edensity:mapfile <map file> -edensity:mapreso
3.2 -edensity:realign no -cutpoint_open 93

```

Refinement of 30S ribosomal subunit

For the 30S ribosomal subunit (3OTO), Rosetta was unable to minimize the entire molecule due to slow scoring caused by its large size, so the molecule was divided into 16 segments. The base-pairing assignment of MC-Annotate served as the criteria for the dividing, in such a way that the base-pairing nucleotides are included in the same segment. The dividing was achieved automatically by a python script, named `create_minimize_segment.py`. The 16 segments were then minimized sequentially from the 5'-end to the 3'-end. To retain all interactions, we also included the nucleotides within 5 Å radius to the segment being minimized as fixed nucleotides during the minimization. The ERRASER rebuilding step was performed in a similar way as mentioned previously. In order to speed up the process, the nucleotide being rebuilt was cut out from the whole structural model together with all nucleotides within 6 Å radius, rebuilt using SWA, and pasted back to the model. The subsequent minimization step was performed in the same way as the first minimization.

Scoring function used in ERRASER

To counter-balance relatively large electron density scoring term, we increased the weight of `fa_rep`, `fa_intra_rep`, `h_bond_sc`, `hbond_sr_bb_sc`, `hbond_lr_bb_sc`, `fa_stack`, `rna_torsion` and `rna_sugar_close`.

Scoring weights for SWA rebuilding:

<code>fa_atr</code>	0.23
<code>fa_rep</code>	4.0
<code>fa_intra_rep</code>	0.8
<code>rna_torsion</code>	80
<code>rna_sugar_close</code>	2.0
<code>hbond_sr_bb_sc</code>	2.6
<code>hbond_lr_bb_sc</code>	10
<code>hbond_sc</code>	10
<code>geom_sol</code>	0.62
<code>ch_bond</code>	0.42
<code>lk_nonpolar</code>	0.32
<code>hack_elec_rna_phos_phos</code>	1.05
<code>fa_stack</code>	1.0
<code>elec_dens_atomwise</code>	5.0
<code>angle_constraint</code>	1.0
<code>atom_pair_constraint</code>	1.0
<code>rna_bulge</code>	1.0
<code>linear_chainbreak</code>	40.0

Scoring weights for minimization:

<code>fa_atr</code>	0.23
<code>fa_rep</code>	4.0
<code>fa_intra_rep</code>	0.8
<code>rna_torsion</code>	80
<code>rna_sugar_close</code>	0.7
<code>hbond_sr_bb_sc</code>	2.6
<code>hbond_lr_bb_sc</code>	10
<code>hbond_sc</code>	10
<code>geom_sol</code>	0.62
<code>ch_bond</code>	0.42
<code>lk_nonpolar</code>	0.32
<code>hack_elec_rna_phos_phos</code>	1.05
<code>fa_stack</code>	1.0
<code>elec_dens_atomwise</code>	5.0
<code>rna_bond_geometry</code>	10.0

PHENIX refinement

PHENIX⁴ (v1.7.1-743) is used for all the refinements performed in this study. We first prepared the starting models downloaded from the PDB for refinement using phenix.ready_set. This step added missing hydrogen atoms into the models and set up constraint files including ligand constraints and metal coordination constraints. The obtained models were inspected manually to remove incorrectly added hydrogen atoms, which is common when the RNA contains modified nucleotides. Because phenix.ready_set does not always generate all the ligand constraints correctly, for ligands that phenix.ready_set cannot handle properly, extra ligand constraint files were extracted from CCP4 monomer library and were modified to make them compatible with PHENIX. Also, we noticed that phenix.ready_set cannot generate proper bond length and bond angle constraints at the linkage between a modified nucleotide and a standard nucleotide in RNA, so these constraints were added manually as well. Finally, for pdb files with TLS (Translation/Libration/Screw)⁵ refinement records, the TLS group information was manually extracted from the pdb files and saved in a separate file for further use in PHENIX.

After all the files for the refinement were ready, a three-step PHENIX refinement was performed. In the first step, because PHENIX cannot read in the TLS refinement data stored in the .pdb files as REMARK, we performed a one-cycle TLS refinement to recover the TLS information (PHENIX saves it into the ANISOU record of each atom). Second, the models were refined by phenix.refine for 4 cycles. At this step, wxu_scale (scale for X-ray/ADP weight) was optimized by PHENIX using a grid search, and other parameters were manually determined based on the criteria described below (Supplementary Table 9). For higher resolution structures a higher wxc_scale (scale for X-ray/Stereochemistry weight) is appropriate. Based on initial tests (on PDB cases 1Q9A and 2HOP, not included in this paper's benchmark since they were used to set parameters), we used the following criteria: wxc_scale = 0.5 for Resolution < 2.1 Å, wxc_scale = 0.1 for 2.1 Å ≤ Resolution < 3 Å, and wxc_scale = 0.05 for Resolution ≥ 3 Å. The ordered_solvent option (auto water updating) was turned on only for structures with a resolution < 2.1 Å. One exception, 2A43, was excluded from ordered_solvent refinement because it gave worse R factor. TLS refinement was turned on only for structures with TLS record in the deposited PDB files. Third, the

models were further refined in phenix.refine for 10 cycles, with all target weights (wxc_scale and wxu_scale) optimized during the run. Other parameters ($ordered_solvent$ and TLS) stayed the same as in the first refinement round. This step was much slower than the second step, but according to the phenix.refine documentation, this is usually good for a final model tune up. Nevertheless, in a few cases we found that the second round of refinement led to worse R factor. In those cases we used the result of the first round as the PHENIX output, and also for further ERRASER remodeling. Empirically, we found that the real-space refinement strategy in PHENIX only gave equal or worse R factor, so it was turned off throughout all the refinement steps in this study.

After the initial refinement, the electron density map was generated from the experimental diffraction data and the PHENIX refined structural model for further ERRASER improvement. We used phenix.maps to create $2mF_{obs}-DF_{calc}$ maps in ccp4 format, and diffraction data used for R_{free} validation was excluded for the map generation to avoid directly fitting to the R_{free} test set during the ERRASER refinement. To avoid the Fourier truncation error due to the missing data, we filled the missing F_{obs} with F_{calc} during the map calculation. The averaged kick map approach was also used to reduce the noise and model bias of the maps⁶.

The final PHENIX refinement, after the Rosetta/ERRASER steps, was similar to the starting refinement described above, with small variations. First, there was no need for an initial TLS refinement since the .pdb files already had this information at this stage. Second, we ran phenix.ready_set again on the ERRASER model to generate metal coordination constraints for refinements, because the new model might have different metal coordination pattern than the starting one. The models were then refined using PHENIX in the same two-step fashion, with the same parameter sets (Supplementary Table 9). Similar to that in the starting PHENIX refinement, the models of the 1st and 2nd step were compared to each other and the one with better R and R_{free} was selected as the final output.

We found that some of the default standard deviations of RNA bond angles were too stringent in PHENIX. In initial tests (on PDB cases 1Q9A and 2HOP, not included in this paper benchmark), these stringent constraints appeared to distort models and led to worse overall geometry, as assessed by MolProbity. Therefore we manually modified the default geometry files for RNA in PHENIX using the parameters developed by Parkinson et al⁷, which is also used in MolProbity as the standard RNA geometry (see below).

Examples of the PHENIX command lines used in this work are listed below.

(1) phenix.ready_set

```
phenix.ready_set 3E5E_combine.pdb
```

(2) one-cycle TLS refinement

```
phenix.refine 2QUS-sf.mtz 2QUS.updated.pdb GTP.cif 2QUS.metal.edits  
2QUS.link.edits tls.params main.number_of_macro_cycles=1 strategy=tls
```

(3) 4-cycle refinement with manual parameter set

```
phenix.refine 2QUS-sf.mtz 2QUS.updated.pdb GTP.cif 2QUS.metal.edits  
2QUS.link.edits tls.params main.number_of_macro_cycles=4 strategy=  
individual_sites+individual_adp+tls+occupancies wxc_scale=0.1  
optimize_wxu=true target_weights.mode=every_macro_cycle
```

(4) 10-cycle refinement with automatically optimized target weight

```
phenix.refine 3E5E-sf.mtz 3E5E_combine_refine_001.pdb 3E5E_combine.metal.edits  
3E5E.link main.number_of_macro_cycles=10  
strategy=individual_sites+individual_adp+occupancies optimize_wxc=true  
optimize_wxu=true target_weights.mode=every_macro_cycle
```

(5) density map creation

```
phenix.maps_1.7.1-743 maps.params  
  
maps.params:  
...  
map {  
  map_type = 2mFo-DFc
```

```

format = xplor *ccp4
file_name = "3iwn_1.ccp4"
kicked = True
fill_missing_f_obs = True
grid_resolution_factor = 0.250000
scale = *sigma volume
region = *selection cell
atom_selection = None
atom_selection_buffer = 3.000000
acentrics_scale = 2.000000
centrics_pre_scale = 1.000000
sharpening = False
sharpening_b_factor = None
exclude_free_r_reflections = True
isotropize = True
resharp_after_isotropize = False
}
...

```

Modified PHENIX geometry files

Location of the files: <PHENIX directory>/chem_data/geostd/rna_dna/

1. chain_link_rna2p.cif:

```

data_link_rna2p
#
loop_
  _chem_link_bond.link_id
  _chem_link_bond.atom_1_comp_id
  _chem_link_bond.atom_id_1
  _chem_link_bond.atom_2_comp_id
  _chem_link_bond.atom_id_2
  _chem_link_bond.type
  _chem_link_bond.value_dist
  _chem_link_bond.value_dist_esd
rna2p  1 O3*  2 P      single      1.607  0.012
loop_
  _chem_link_angle.link_id
  _chem_link_angle.atom_1_comp_id
  _chem_link_angle.atom_id_1
  _chem_link_angle.atom_2_comp_id
  _chem_link_angle.atom_id_2
  _chem_link_angle.atom_3_comp_id
  _chem_link_angle.atom_id_3
  _chem_link_angle.value_angle
  _chem_link_angle.value_angle_esd
rna2p  1 O3*  2 P      2 O5*    104.000  1.900
rna2p  1 O3*  2 P      2 O1P    107.400  3.200
rna2p  1 O3*  2 P      2 O2P    108.300  3.200

```

```

rna2p    1 C3*    1 O3*    2 P    119.700    1.200
loop_
_chem_link_tor.link_id
_chem_link_tor.id
_chem_link_tor.atom_1_comp_id
_chem_link_tor.atom_id_1
_chem_link_tor.atom_2_comp_id
_chem_link_tor.atom_id_2
_chem_link_tor.atom_3_comp_id
_chem_link_tor.atom_id_3
_chem_link_tor.atom_4_comp_id
_chem_link_tor.atom_id_4
_chem_link_tor.value_angle
_chem_link_tor.value_angle_esd
_chem_link_tor.period
rna2p    epsilon  1 C4*    1 C3*    1 O3*    2 P    -100.00  30.0 3
rna2p    zeta    1 C3*    1 O3*    2 P    2 O5*    145.00  30.0 3
rna2p    alpha   1 O3*    2 P    2 O5*    2 C5*    165.00  20.0 3
#

```

2. chain_link_rna3p.cif:

```

data_link_rna3p
#
loop_
_chem_link_bond.link_id
_chem_link_bond.atom_1_comp_id
_chem_link_bond.atom_id_1
_chem_link_bond.atom_2_comp_id
_chem_link_bond.atom_id_2
_chem_link_bond.type
_chem_link_bond.value_dist
_chem_link_bond.value_dist_esd
rna3p    1 O3*    2 P    single    1.607    0.012
loop_
_chem_link_angle.link_id
_chem_link_angle.atom_1_comp_id
_chem_link_angle.atom_id_1
_chem_link_angle.atom_2_comp_id
_chem_link_angle.atom_id_2
_chem_link_angle.atom_3_comp_id
_chem_link_angle.atom_id_3
_chem_link_angle.value_angle
_chem_link_angle.value_angle_esd
rna3p    1 O3*    2 P    2 O5*    104.000    1.900
rna3p    1 O3*    2 P    2 O1P    107.400    3.200
rna3p    1 O3*    2 P    2 O2P    108.300    3.200
rna3p    1 C3*    1 O3*    2 P    119.700    1.200
loop_
_chem_link_tor.link_id

```

```

_chem_link_tor.id
_chem_link_tor.atom_1_comp_id
_chem_link_tor.atom_id_1
_chem_link_tor.atom_2_comp_id
_chem_link_tor.atom_id_2
_chem_link_tor.atom_3_comp_id
_chem_link_tor.atom_id_3
_chem_link_tor.atom_4_comp_id
_chem_link_tor.atom_id_4
_chem_link_tor.value_angle
_chem_link_tor.value_angle_esd
_chem_link_tor.period
rna3p  epsilon  1 C4*   1 C3*   1 O3*   2 P      -150.00  30.0  3
rna3p  zeta    1 C3*   1 O3*   2 P      2 O5*   172.00  30.0  3
rna3p  alpha   1 O3*   2 P      2 O5*   2 C5*   300.00  20.0  3
#

```

3. mod_rna2p.cif:

```

data_mod_rna2p
#
loop_
_chem_mod_bond.mod_id
_chem_mod_bond.function
_chem_mod_bond.atom_id_1
_chem_mod_bond.atom_id_2
_chem_mod_bond.new_type
_chem_mod_bond.new_value_dist
_chem_mod_bond.new_value_dist_esd
rna2p change P O5* coval 1.593 0.010
rna2p change C1* C2* coval 1.528 0.010
rna2p change C2* C3* coval 1.525 0.011
rna2p change C3* C4* coval 1.524 0.011
rna2p change C3* O3* coval 1.423 0.014
rna2p change C4* C5* coval 1.510 0.013
rna2p change C4* O4* coval 1.453 0.012
rna2p change O4* C1* coval 1.414 0.012
rna2p change C5* O5* coval 1.440 0.016
rna2p change C2* O2* coval 1.413 0.013
rna2p change N9 C1* coval 1.460 0.011
loop_
_chem_mod_angle.mod_id
_chem_mod_angle.function
_chem_mod_angle.atom_id_1
_chem_mod_angle.atom_id_2
_chem_mod_angle.atom_id_3
_chem_mod_angle.new_value_angle
_chem_mod_angle.new_value_angle_esd
rna2p change N9 C1* O4* 108.2 1.0
rna2p change N9 C1* C2* 113.4 1.6

```

```

rna2p change N1 C1* O4* 108.2 1.0
rna2p change N1 C1* C2* 113.4 1.6
rna2p change O4* C1* C2* 106.4 1.4
rna2p change C1* C2* C3* 101.5 0.9
rna2p change C2* C3* C4* 102.7 1.0
rna2p change C2* C3* O3* 111.0 2.8
rna2p change O3* C3* C4* 110.6 2.6
rna2p change C3* C4* C5* 115.5 1.5
rna2p change C3* C4* O4* 105.5 1.4
rna2p change O4* C4* C5* 109.2 1.4
rna2p change C4* O4* C1* 109.6 0.9
rna2p change C4* C5* O5* 110.2 1.4
rna2p change C1* C2* O2* 110.6 3.0
rna2p change O2* C2* C3* 113.3 2.9
rna2p change C5* O5* P 120.9 1.6
rna2p change O5* P O1P 108.1 2.9
rna2p change O1P P O2P 119.6 1.5
rna2p change O5* P O2P 108.3 2.7
loop_
  _chem_mod_tor.mod_id
  _chem_mod_tor.function
  _chem_mod_tor.id
  _chem_mod_tor.atom_id_1
  _chem_mod_tor.atom_id_2
  _chem_mod_tor.atom_id_3
  _chem_mod_tor.atom_id_4
  _chem_mod_tor.new_value_angle
  _chem_mod_tor.new_value_angle_esd
  _chem_mod_tor.new_period
rna2p change beta P O5* C5* C4* 170.0 40.0 1
rna2p change gamma O5* C5* C4* C3* 55.0 15.0 3
rna2p change delta C5* C4* C3* O3* 147.0 8.0 1
rna2p change nu0 C4* O4* C1* C2* 339.0 8.0 1
rna2p change nu1 O4* C1* C2* C3* 35.0 8.0 1
rna2p change nu2 C1* C2* C3* C4* 325.0 8.0 1
rna2p change nu3 C2* C3* C4* O4* 24.0 8.0 1
rna2p change realnu4 C3* C4* O4* C1* 358.0 8.0 1
rna2p change wasnu4 C5* C4* O4* C1* 123.0 8.0 1

```

4. mod_rna3p.cif:

```

data_mod_rna3p
#
loop_
  _chem_mod_bond.mod_id
  _chem_mod_bond.function
  _chem_mod_bond.atom_id_1
  _chem_mod_bond.atom_id_2
  _chem_mod_bond.new_type
  _chem_mod_bond.new_value_dist

```

```

_chem_mod_bond.new_value_dist_esd
rna3p change P O5* coval 1.593 0.015
rna3p change C1* C2* coval 1.529 0.015
rna3p change C2* C3* coval 1.523 0.015
rna3p change C3* C4* coval 1.521 0.015
rna3p change C3* O3* coval 1.417 0.015
rna3p change C4* C5* coval 1.508 0.015
rna3p change C4* O4* coval 1.451 0.015
rna3p change O4* C1* coval 1.412 0.015
rna3p change C5* O5* coval 1.420 0.015
rna3p change C2* O2* coval 1.420 0.015
rna3p change N9 C1* coval 1.475 0.015

```

loop_

```

_chem_mod_angle.mod_id
_chem_mod_angle.function
_chem_mod_angle.atom_id_1
_chem_mod_angle.atom_id_2
_chem_mod_angle.atom_id_3
_chem_mod_angle.new_value_angle
_chem_mod_angle.new_value_angle_esd
rna3p change N9 C1* O4* 108.5 1.000
rna3p change N9 C1* C2* 112.0 1.000
rna3p change N1 C1* O4* 108.5 1.000
rna3p change N1 C1* C2* 112.0 1.000
rna3p change O4* C1* C2* 107.6 1.000
rna3p change C1* C2* C3* 101.3 1.000
rna3p change C2* C3* C4* 102.6 1.000
rna3p change C2* C3* O3* 113.7 1.000
rna3p change O3* C3* C4* 113.0 1.000
rna3p change C3* C4* C5* 116.0 1.000
rna3p change C3* C4* O4* 104.0 1.000
rna3p change O4* C4* C5* 109.8 1.000
rna3p change C4* O4* C1* 109.9 1.000
rna3p change C4* C5* O5* 111.5 1.000
rna3p change C1* C2* O2* 108.4 1.000
rna3p change O2* C2* C3* 110.7 1.000
rna3p change C5* O5* P 120.9 1.000
rna3p change O5* P O1P 110.7 1.000
rna3p change O1P P O2P 119.6 1.000
rna3p change O5* P O2P 110.7 1.000

```

loop_

```

_chem_mod_tor.mod_id
_chem_mod_tor.function
_chem_mod_tor.id
_chem_mod_tor.atom_id_1
_chem_mod_tor.atom_id_2
_chem_mod_tor.atom_id_3
_chem_mod_tor.atom_id_4
_chem_mod_tor.new_value_angle
_chem_mod_tor.new_value_angle_esd
_chem_mod_tor.new_period

```

```

rna3p change beta P O5* C5* C4* 170.0 40.0 1
rna3p change gamma O5* C5* C4* C3* 55.0 15.0 3
rna3p change delta C5* C4* C3* O3* 82.0 8.0 1
rna3p change nu0 C4* O4* C1* C2* 3.0 8.0 1
rna3p change nu1 O4* C1* C2* C3* 335.0 8.0 1
rna3p change nu2 C1* C2* C3* C4* 36.0 8.0 1
rna3p change nu3 C2* C3* C4* O4* 325.0 8.0 1
rna3p change realnu4 C3* C4* O4* C1* 20.0 8.0 1
rna3p change wasnu4 C5* C4* O4* C1* 145.0 8.0 1

```

References

1. DiMaio, F. et al. Improved molecular replacement by density- and energy-guided protein structure optimization. *Nature* **473**, 540-543 (2011).
2. DiMaio, F., Tyka, M.D., Baker, M.L., Chiu, W. & Baker, D. Refinement of Protein Structures into Low-Resolution Density Maps Using Rosetta. *J. Mol. Biol.* **392**, 181-190 (2009).
3. Mandell, D.J., Coutsias, E.A. & Kortemme, T. Sub-angstrom accuracy in protein loop reconstruction by robotics-inspired conformational sampling. *Nat. Methods* **6**, 551-552 (2009).
4. Adams, P.D. et al. PHENIX: a comprehensive Python-based system for macromolecular structure solution. *Acta Cryst. D* **66**, 213-221 (2010).
5. Winn, M.D., Isupov, M.N. & Murshudov, G.N. Use of TLS parameters to model anisotropic displacements in macromolecular refinement. *Acta Cryst. D* **57**, 122-133 (2001).
6. Praznikar, J., Afonine, P.V., Guncar, G., Adams, P.D. & Turk, D. Averaged kick maps: less noise, more signal...and probably less bias. *Acta Cryst. D* **65**, 921-931 (2009).
7. Parkinson, G., Vojtechovsky, J., Clowney, L., Brunger, A.T. & Berman, H.M. New parameters for the refinement of nucleic acid-containing structures. *Acta Cryst. D* **52**, 57-64 (1996).

Supplementary Table 1. Clashscore of the benchmark assessed by MolProbity

PDB ID	PDB	PHENIX	RNABC/ PHENIX	RCrane/ PHENIX	ERRASER /PHENIX
2A43	1.19	1.19	2.38	1.19	1.19
3DIL	1.40	5.6	7.52	7.35	5.95
2GDI	4.98	8.81	11.11	6.32	5.17
2QUS	12.97	15.21	18.11	13.64	8.72
2OIU	8.48	17.82	22.6	20.65	6.09
2CKY	20.01	27.14	17.83	17.04	8.12
2GIS	42.85	30.7	31.66	40.29	21.75
3E5E	5.09	10.74	13.57	21.48	7.91
3F2Q	9.47	5.85	7.24	8.08	3.34
3R4F	49.62	93.1	49.62	46.31	27.84
3P49	17.56	20.84	30.84	26.98	20.13
1U8D	14.02	9.25	13.46	9.25	11.35
1Y27	6.82	13.63	7.27	3.63	6.36
3MXH	8.45	6.89	10	10.67	7.56
3IWN	56.02	57.79	61.23	34.72	22.3
Average	17.26	21.64	20.30	17.84	10.92
Equal or better than PDB		5 / 15	5 / 15	8 / 15	11 / 15

Supplementary Table 2. Potentially incorrect sugar puckers and outlier conformers of the benchmark assessed

by MolProbability

PDB ID	Potentially incorrect puckers					Outlier conformers				
	PDB	PHENIX	RNABC/ PHENIX	RCrane/ PHENIX	ERRASER /PHENIX	PDB	PHENIX	RNABC/ PHENIX	RCrane/ PHENIX	ERRASER /PHENIX
2A43	0	0	0	0	0	1	1	1	2	1
3DIL	4	2	3	3	0	18	13	15	15	13
2GDI	8	3	3	2	2	23	18	18	16	12
2QUS	9	6	6	2	0	35	29	29	19	15
2OIU	6	3	2	2	0	29	24	23	14	7
2CKY	18	9	6	3	2	64	53	44	28	17
2GIS	8	7	6	4	0	21	19	17	23	9
3E5E	2	1	1	0	0	6	6	6	6	3
3F2Q	3	2	2	2	0	22	16	16	10	7
3R4F	5	5	2	1	0	16	25	22	8	9
3P49	19	11	12	8	4	73	56	59	30	28
1U8D	3	2	2	1	0	4	4	3	4	0
1Y27	4	2	2	0	0	13	13	13	3	7
3MXH	1	1	1	0	1	8	7	7	9	8
3IWN	23	17	12	7	2	52	67	76	28	26
Average	7.53	4.73	4.00	2.33	0.73	25.67	23.40	23.27	14.33	11.07
Equal or better than PDB		15 / 15	15 / 15	15 / 15	15 / 15		13 / 15	13 / 15	12 / 15	15 / 15

Supplementary Table 3. Outlier bond lengths and bond angles of the benchmark assessed by MolProbity

PDB ID	Outlier angle (%)					Outlier bonds (%)				
	PDB	PHENIX	RNABC/ PHENIX	RCrane/ PHENIX	ERRASER /PHENIX	PDB	PHENIX	RNABC/ PHENIX	RCrane/ PHENIX	ERRASER /PHENIX
2A43	34.62	0	3.85	3.85	0	0	0	0	0	0
3DIL	6.32	2.3	2.3	5.17	1.72	0	0	0	1.15	0
2GDI	6.96	0.63	0.63	5.06	0.63	0	0	0	0.63	0
2QUS	35.29	1.47	0.74	2.94	0	2.21	0	0	0	0
2OIU	45.77	2.82	7.04	6.34	0	7.04	0	0	0	0
2CKY	57.79	1.95	0	0.65	0	1.3	0	0	0	0
2GIS	9.57	1.06	1.06	5.32	0	0	0	0	0	0
3E5E	21.15	0	0	1.92	0	1.92	0	0	0	0
3F2Q	6.48	0.93	0.93	2.78	0.93	0	0	0	0	0
3R4F	7.58	1.52	0	1.52	0	0	0	0	0	0
3P49	18.34	1.18	0.59	4.14	0	0	0	0	0	0
1U8D	14.93	4.48	1.49	0	1.49	1.49	0	0	0	0
1Y27	11.94	2.99	0	2.99	0	1.49	0	0	0	0
3MXH	2.2	0	0	1.1	0	0	0	0	0	0
3IWN	9.14	12.9	9.14	3.23	0	0	0	0	0	0
Average	19.21	2.28	1.85	3.13	0.32	1.03	0.00	0.00	0.12	0.00
Equal or better than PDB		14 / 15	15 / 15	15 / 15	15 / 15		15 / 15	15 / 15	13 / 15	15 / 15

Supplementary Table 4. Number of base-pairs identified by MC-Annotate

PDB ID	PDB	PHENIX	RNABC/ PHENIX	RCrane/ PHENIX	ERRASER/ PHENIX
2A43	12	12	12	12	12
3DIL	88	88	88	89	88
2GDI	70	71	70	70	70
2QUS	52	52	52	52	50
2OIU	60	60	60	59	63
2CKY	70	65	68	64	67
2GIS	40	39	38	38	37
3E5E	20	20	21	21	21
3F2Q	43	45	45	45	44
3R4F	25	21	21	21	24
3P49	44	42	49	49	60
1U8D	31	32	32	32	31
1Y27	36	35	36	34	35
3MXH	38	39	40	39	39
3IWN	64	63	64	68	76
Average	46.20	45.60	46.40	46.20	47.80
Equal or better than PDB		9 / 15	12 / 15	10 / 15	10 / 15

Supplementary Table 5. R factors of the benchmark

PDB ID	PDB (Deposited)	PDB (PHENIX calculated)	PHENIX	RNABC/ PHENIX	RCrane/ PHENIX	ERRASER /PHENIX
2A43	0.114	0.135	0.119	0.125	0.126	0.123
3DIL	0.194	0.188	0.173	0.174	0.177	0.173
2GDI	0.210	0.207	0.194	0.200	0.195	0.196
2QUS	0.191	0.192	0.199	0.203	0.201	0.202
2OIU	0.206	0.204	0.195	0.191	0.193	0.207
2CKY	0.191	0.195	0.165	0.172	0.174	0.178
2GIS	0.266	0.264	0.217	0.214	0.206	0.219
3E5E	0.222	0.224	0.195	0.197	0.202	0.196
3F2Q	0.202	0.207	0.207	0.210	0.207	0.209
3R4F	0.239	0.252	0.219	0.234	0.236	0.219
3P49	0.284	0.283	0.219	0.212	0.218	0.218
1U8D	0.178	0.188	0.178	0.178	0.184	0.178
1Y27	0.233	0.235	0.217	0.226	0.226	0.220
3MXH	0.203	0.239	0.198	0.198	0.200	0.195
3IWN	0.222	0.223	0.197	0.195	0.218	0.221
Average Drop ^a			-0.023	-0.020	-0.018	-0.019
Equal or better than PDB			14 / 15	13 / 15	14 / 15	12 / 15
Within 0.005 of PDB or better			14 / 15	14 / 15	14 / 15	14 / 15

^a compared to PDB values.

Supplementary Table 6. R_{free} factors of the benchmark

PDB ID	PDB (Deposited)	PDB (PHENIX calculated)	PHENIX	RNABC/ PHENIX	RCrane/ PHENIX	ERRASER /PHENIX
2A43	0.190	0.183	0.157	0.159	0.163	0.158
3DIL	0.229	0.220	0.207	0.203	0.207	0.206
2GDI	0.241	0.238	0.232	0.233	0.234	0.235
2QUS	0.253	0.265	0.271	0.268	0.270	0.266
2OIU	0.238	0.234	0.237	0.235	0.237	0.236
2CKY	0.250	0.250	0.243	0.241	0.245	0.234
2GIS	0.289	0.269	0.260	0.261	0.264	0.262
3E5E	0.259	0.254	0.250	0.250	0.273	0.253
3F2Q	0.243	0.265	0.264	0.266	0.273	0.266
3R4F	0.271	0.290	0.278	0.292	0.293	0.277
3P49	0.310	0.302	0.278	0.280	0.274	0.271
1U8D	0.228	0.225	0.211	0.213	0.213	0.211
1Y27	0.264	0.265	0.280	0.280	0.268	0.270
3MXH	0.239	0.287	0.257	0.256	0.258	0.252
3IWN	0.292	0.294	0.291	0.293	0.291	0.292
Average Drop ^a			-0.008	-0.007	-0.005	-0.010
Equal or better than PDB			12 / 15	10 / 15	9 / 15	11 / 15
Within 0.005 of PDB or better			13 / 15	14 / 15	13 / 15	15 / 15

^a compared to PDB values.

Supplementary Table 7. Similarity analysis for models of the same or similar sequences

Chain 1	Chain 2	Similar residues (%) ^a					Similar puckers (%) ^b				
		PDB	PHENIX	RNABC/ PHENIX	RCrane/ PHENIX	ERRASER /PHENIX	PDB	PHENIX	RNABC/ PHENIX	RCrane/ PHENIX	ERRASER /PHENIX
2GDI_1	2GDI_2	79.49	87.18	84.62	83.33	88.46	97.44	100.00	100.00	98.72	97.44
2OIU_1	2OIU_2	42.25	45.07	49.30	61.97	66.20	87.32	94.37	94.37	94.37	95.77
2QUS_1	2QUS_2	63.24	72.06	72.06	83.82	82.35	92.65	91.18	92.65	94.12	94.12
3IWN_1	3IWN_2	50.65	35.06	38.96	59.74	66.23	94.81	93.51	90.91	90.91	96.10
3IWN_1	3MXH	53.25	51.95	51.95	71.43	64.94	85.71	89.61	92.21	90.91	93.51
3IWN_2	3MXH	46.75	45.45	48.05	50.65	57.14	81.82	90.91	90.91	90.91	89.61
3P49_1	3P49_2	34.21	34.21	34.21	68.42	68.42	84.21	94.74	92.11	97.37	94.74
2CKY_1	2CKY_2	59.74	62.34	61.04	84.42	79.22	90.91	98.70	97.40	98.70	97.40
1U8D	1Y27	68.85	68.85	77.05	93.44	85.25	95.08	93.44	100.00	100.00	98.36
Average		55.38	55.80	57.47	73.03	73.13	89.99	94.05	94.51	95.11	95.23
Equal or better than PDB			6 / 9	7 / 9	9 / 9	9 / 9		6 / 9	8 / 9	8 / 9	9 / 9

^a Nucleotide pair in which the differences between all torsion angles are smaller than 40°.

^b Nucleotide pair in which the difference between δ angle is smaller than 20°.

Supplementary Table 8. Torsional RMSDs (in degrees) for models of the same or similar sequences

Chain 1	Chain 2	PDB	PHENIX	RNABC/ PHENIX	RCrane/ PHENIX	ERRASER /PHENIX
2GDI_1	2GDI_2	25.07	23.45	23.56	24.12	24.56
2OIU_1	2OIU_2	44.46	42.14	42.38	38.99	35.24
2QUS_1	2QUS_2	46.24	43.23	42.50	25.82	29.27
3IWN_1	3IWN_2	42.62	45.22	44.63	44.89	38.58
3IWN_1	3MXH	48.08	46.04	44.26	37.91	40.22
3IWN_2	3MXH	51.97	50.86	49.10	44.75	42.79
3P49_1	3P49_2	50.40	49.60	49.78	34.35	36.10
2CKY_1	2CKY_2	32.13	32.89	32.50	25.14	30.73
1U8D	1Y27	36.14	35.55	33.59	17.27	23.69
Average		41.90	41.00	40.25	32.58	33.46
Equal or better than PDB			7 / 9	7 / 9	8 / 9	9 / 9

RMSD is calculated between all the torsion angles in the model pair.

Supplementary Table 9. PHENIX refinement parameters

PDB ID	Resolution (Å)	wxc_scale	TLS refinement	ordered_solvent
2A43	1.34	0.50	No	No
3DIL	1.9	0.50	No	Yes
2GDI	2.05	0.50	No	Yes
2QUS	2.4	0.10	Yes	No
2OIU	2.6	0.10	Yes	No
2CKY	2.9	0.10	No	No
2GIS	2.9	0.10	No	No
3E5E	2.9	0.10	Yes	No
3F2Q	2.95	0.10	Yes	No
3R4F	3.5	0.05	No	No
3P49	3.55	0.05	Yes	No
1U8D	1.95	0.50	No	Yes
1Y27	2.4	0.10	Yes	No
3MXH	2.3	0.10	Yes	No
3IWN	3.2	0.05	No	No
3OTO	3.69	0.05	Yes	No

Supplementary Figure 1. Flow chart of the ERRASER/PHENIX pipeline. The ERRASER steps are enclosed in red.

